Polym. Korea, Vol. 46, No. 4, pp. 529-535 (2022)
https://doi.org/10.7317/pk.2022.46.4.529

ISSN 0379-153X(Print)
ISSN 2234-8077(Online)

수산화마그네슘으로 충전된 폴리(4-메틸-1-펜텐) 기반 복합체의 열적, 기계적, 전기적 및 난연 특성

김상범†ID · 정영섭* · 박은수*,†ID
한국생산기술연구원, *(주)인테크놀로지
(2022년 4월 14일 접수, 2022년 5월 23일 수정, 2022년 5월 30일 채택)

Thermal, Mechanical, Electrical, and Flame Retardant Properties of Poly(4-methyl-1-pentene) based Composites Filled with Magnesium Hydroxide

Sang Bum Kim†ID, Young Seob Jong*, and Eun-Soo Park*,†ID
Korea Institute of Industrial Technology, 89 Yangdaegiro-gil, Ipjang-myeon, Seobuk-gu, Chungcheongnam-do, 31056, Korea
**Intechnology Co., Ltd., 861-46, Poseungjangan-ro, Jang-an-ri, Jangan-myeon, Hwaseong-si, Gyeonggi-do, 18586, Korea*
(Received April 14, 2022; Revised May 23, 2022; Accepted May 30, 2022)

초록: 비할로겐계 난연제인 수산화마그네슘(MDH)으로 충전된 폴리(4-메틸-1-펜텐) (PMP)을 기반으로 한 복합체를 제작하여 열적, 기계적, 전기적 및 미세구조 연구를 진행하였다. 제작된 복합체의 전자선(EB) 조사량에 따른 이들 특성 변화 또한 연구 하였다. MDH의 충전은 PMP/PP의 화재 성능과 열적 안정성을 현저히 향상시켰으나, MDH를 너무 많이 충전시키면 PMP/PP/MDH 복합체를 취화시켜 결과적으로 작은 변형에서도 파괴를 일으켰다. 절연저항 시험을 통해 10 wt%의 MDH까지 증가하다가 이후 감소하는 PMP/PP/MDH 복합체의 인장 강도 변화와 동일한 경향이 있음을 확인하였다. 반면 가교제 없이 시행된 전자선 조사는 상기한 특성들을 실질적으로 감소시켰다.

Abstract: Poly(4-methyl-1-pentene) (PMP) based composite filled with magnesium hydroxide (MDH) as a non-halogenated flame retardant was prepared and its thermal, mechanical, electrical, and morphological properties were studied. Changes in the properties of the prepared composites as a function of electron beam (EB) irradiation were also investigated. The results show that the incorporation of MDH significantly enhanced the fire performance and thermal stability of PMP/PP. However, excessive addition of MDH made the PMP/PP/MDH composites brittle, and consequently, fractures occurred at small deformations. The insulation resistance test confirms that there is the same change tendency as the tensile strength of PMP/PP/MDH composites which increases up to 10 wt% of MDH and then decrease thereafter. However, EB irradiation without a crosslinking agent substantially degrades these properties.

Keywords: flexible, insulation, magnesium hydroxide, composite, flame retardant.

Introduction

Hydrogen fuel cell vehicles (HFCV) have attracted attention as a solution to the energy crisis and exhaust gas problems of vehicles. Governments around the world have identified the development of standards and regulations as one of the key requirements for HFCV commercialization.[1] Development of a technique for safety assessment of HFCV includes four tasks, research for regulation system/policy, vehicle operation safety, hydrogen safety and protection against high-voltage. HFCVs have a complex high voltage electrical system that includes highly specialized power cables. They are manually assembled in the cable harness process and then installed on the vehicle.[2] As a result, installation efficiency, accuracy, and workload in cable harness depend primarily on the flexibility of the cables used. Not only can they maintain their properties up to 150 °C, but they are also fire-retardant, with no corrosive or toxic gases at fires.

Poly(4-methyl-1-pentene) (PMP) is a polyolefin resin with a linear isotactic structure that combines relatively high thermal stability, chemical resistance, and an extremely low dielectric constant and density.[3,4] Commercially produced grades are primarily copolymers. Therefore, PMP and its copolymers have great potential for electrical insulation applications that require

†To whom correspondence should be addressed.
sbkim@kitech.re.kr, ORCID 0000-0002-4021-6709
t2phage@hitel.net, ORCID 0000-0002-4150-7401

high thermal stability and low dielectric constant as well as lightweight.[5]

The focus of this study is to develop a highly flexible and thermally stable insulating material for HFCV cables, which is a bottleneck that restricts the development of cables with small bending stiffness. A PMP-based composite filled with magnesium hydroxide (MDH) as a non-halogenated flame retardant was prepared and their thermal, mechanical, electrical and flame retardant properties were studied. Change in the properties of the composites as a function of the electron beam (EB)-irradiation was also investigated.

Experimental

Materials. MDH (PUREMAG® FNM) was purchased Tateho Chemical Industries Co., Ltd., Tokyo, Japan. Poly(4-methyl pentene-1) (PMP): TPX DX 560M (supplied by Kangshin Industrial Co., Ltd., Korea) was used for the preparation of polymer composites. The PMP used in this study was a melt extrudable 4-methyl-1-pentene based copolymer containing 30 wt% polypropylene (PP), which improves the extrudability and elongation of PMP.

Instrumentation. The morphology of the MDH was measured using a JEOL JEM-1220 model (Japan) transmission electron microscope (TEM) with an accelerating voltage of 120 kV.

The surface of the cryogenically fractured composite sample in liquid nitrogen was measured using a Hitachi S-4300 model (Japan) scanning electron microscope (SEM) at an accelerating voltage of ~15 kV. To improve resolution, the surface of the sample was coated with platinum using an SPI sputter coater.

The limiting oxygen index (LOI) of the bar specimens (120 × 15 × 2 mm^3) was measured by a DYP-41 LOI instrument (DADYOUNTNS Co., Ltd., Korea) according to ASTM D2863.[6]

The tensile test of the dumbbell specimen (IEC 60811-1-1 type) was performed at a crosshead speed of 50 mm/min using a DEC-A500TC (Dawha Test Machine, Korea) universal testing machine (UTM).

The thermal properties of the samples were determined by differential scanning calorimetry (DSC 7, Perkin-Elmer, USA). Thermal history of the composite was removed by scanning from 20 °C to 300 °C at a heating rate of 20 °C/min (first-scan). After the sample was cooled to room temperature at a rate of -10 °C/min (crystallization), it was reheated from 20 °C to 300 °C (second-scan) to obtain a DSC thermogram.

The thermal stability of the PMP/PP/MDH composites was determined by on a TGA7 (Perkin Elmer, USA) thermogravimetric analyzer. Thermogram curves were obtained under a nitrogen atmosphere by scanning from 20 °C to 800 °C at a heating rate of 20 °C/min.

The insulation resistance (IR) of the composite films (25 mm diameter) was detected by a TeraOhm 5 kV meter (Metrel, USA) according to ASTM D 257.[7] The current stress was 2.5 kV at 20 °C and the charge time of measurements was 30 s.

Preparation of PMP/PP/MDH Composite Film. PMP/PP/MDH composites were melt-blended with MDH loadings of from 10 to 50 wt% in a twin-screw extruder (Twin AT60, Germany) using a temperature setting of Rear zone: 225 °C, Second zone: 240 °C, Forward zone: 240 °C, Adapter: 255 °C, and Die: 260 °C and a mixing rate of 10 kg/h, and then cut into pellet form by a pelletizer. Prepared pellets were dried in an oven at 100 °C for 24 h to remove moisture from them. The film samples were prepared by pressing the composites pellets on a hot press at 260 °C for 10 min and quickly immersing them in water. They were dried at 100 °C for 24 h.

EB-irradiation of Hot-pressed Film. EB irradiation of the hot-pressed films was performed at room temperature at a speed of 1 m/min using an ELV 4 accelerator (EB Tech Co., Ltd., Korea). The applied irradiation dose was varied from 10 Mrad to 40 Mrad by increasing the number of passes. The doses were verified using a cellulose triacetate dosimeter film based on ISO/ASTM51650.[8]

Results and Discussion

Preparation of PMP/PP/MDH Composites. The morphology and size of the MDH particles were analyzed by TEM. As shown in Figure 1, the average size of the MDH with irregularly shaped particles was approximately 300 nm. However, some of the particles were micron-sized. In the case of using MDH for a polymer resin with inherently low flame retardancy, the amount required to satisfy the fire performance requirements is about 30-65 wt%. The PMP/PP/MDH com-

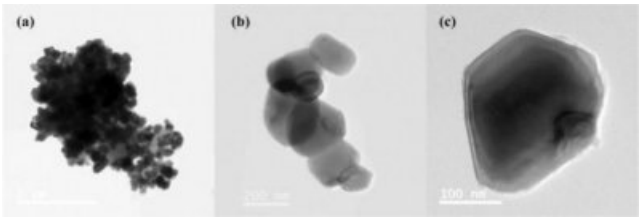

Figure 1. TEM micrographs of the MDH particles.

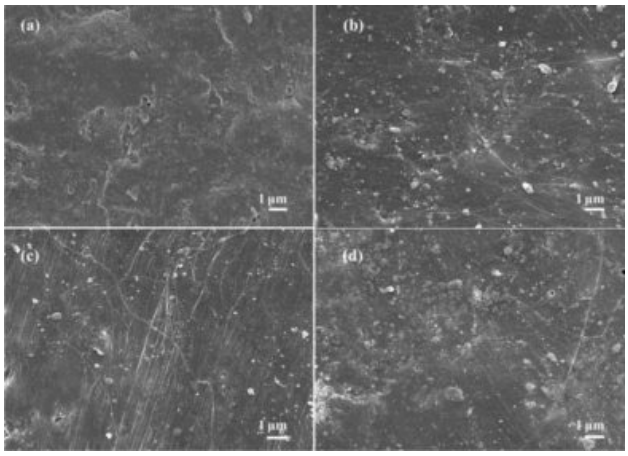

Figure 2. Cryogenic-fractured surface of the PMP/PP/MDH composites (MDH content (a) 10 wt%; (b) 30 wt%; (c) 40 wt%; (d) 50 wt%).

posites were prepared with MDH loadings ranging from 10 wt% to 50 wt% using a twin-screw extruder.

To evaluate changes in the morphology and distribution of the filler particles in the polymer matrix, cryogenic-fractured surfaces of the film samples were observed through SEM. The cryogenic-fractured surfaces of PMP/PP have moderately smooth fractured surface with small voids.[5] From Figure 2, smooth fracture surfaces without necking were observed in all PMP/PP/MDH composites. Examination of the images suggests that 10 wt% MDH (Figure 2(a)) in the matrix ensures uniform dispersion. Increase of MDH content from 30 to 50 wt% (Figure 2(b)-(d)) results in large agglomerates of non-uniform shapes and sizes. Inorganic fillers have a great tendency to agglomerate and the probability increases as the particle size decreases. These agglomerated particles can become stress concentration points and affect the final performance of the composite.[9]

Fire and Tensile Behavior of Composites. The tensile and LOI test results of the PMP/PP/MDH composites with different MDH contents are summarized in Table 1 and the stress-strain plots are obtained from the tensile test of composites as shown in Figure 3. In Table 1, the abbreviation of the sample code, for example, PMP/PP/MDH10wt% means that the content of MDH in PMP/PP is 10 wt%.

The flame retardancy of the unfilled and MDH filled PMP/PP samples was characterized by LOI measurements. The incorporation of MDH enhanced the fire resistance of PMP/PP. The LOI of PMP/PP/MDH10wt% and PMP/PP/MDH50wt% were 19.3% and 29.7%, which is an increase of approximately 8.4% and 40.0%, respectively than that of unfilled PMP/PP (17.8%). Nevertheless, the low rise in the LOI value is likely due to the low dispersibility of the MDH particles. In a fire, MDH decomposes to form a char layer that inhibits heat transfer between the molten polymer and combustion surface and the movement of decomposition materials.[10] However, if the content of MDH is higher than the critical value, the particles of MDH agglomerate and the degree of dispersion is lowered (Figure 2(c) and 2(d)), so that a dense char layer cannot be formed.[10]

Table 1. Tensile and LOI Test Results

Sample code	Tensile properties		LOI (%)
	Tensile strength (MPa)	Elongation at break (%)	
PMP/PP	14.5 ± 0.4	444 ± 16	17.8
PMP/PP/MDH10wt%	14.8 ± 1.0	398 ± 72	19.3
PMP/PP/MDH20wt%	13.2 ± 0.1	327 ± 40	21.2
PMP/PP/MDH30wt%	12.5 ± 0.9	242 ± 31	23.5
PMP/PP/MDH40wt%	10.4 ± 0.4	197 ± 38	26.4
PMP/PP/MDH50wt%	9.2 ± 1.5	149 ± 13	29.7

The tensile strength of the PMP/PP/MDH composite increased up to 10 wt% MDH, whereas further increments resulted in a significant decrease in tensile strength. The tensile strength of PMP/PP/MDH10wt% was increased by 2.1% to 14.8 MPa compared to the unfilled PMP/PP (14.5 MPa). On the contrary, addition of 50 wt% of MDH decreased the tensile strength of PMP by 37.8% than that of addition of 10 wt% (Table 1). This significant reduction in the tensile strength of the composites at 50 wt% MDH loading may be due to the inevitable aggregation of MDH particles (Figure 2(d)). They form the weakest point in the composite leading to premature tensile failure. The elongation at break of the PMP/PP/MDH composites gradually decreased as the MDH content increased. For PMP/PP/MDH10wt% and PMP/PP/MDH50wt%, the elongation at break is measured as 398 and 149%, which is 1.12 and 2.98 times lower than that of unfilled PMP/PP, respectively. This indicates the interference of the filler in the mobility or deformability of the matrix.[9]

Figure 3 displays the stress-strain plot of the PMP/PP/MDH composite. The stress-strain curves of PMP/PP and its composites show the necking and cold-drawing seen in typical semi-crystalline polymers.[9,11] The yield was evident, followed by strain softening and subsequent strain hardening. At first stress and strain rise in a linear relationship up to yield, at which point necking begins. Necking proceeded along the

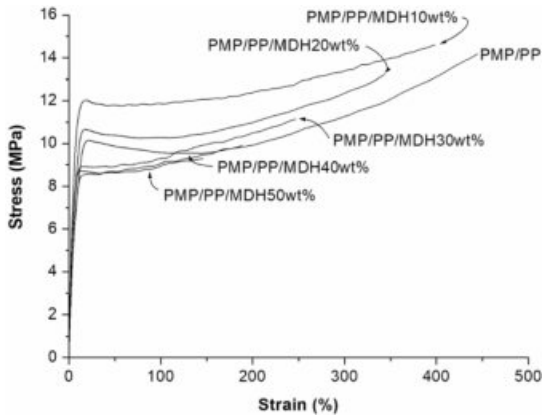

Figure 3. Stress-strain plot of the composites.

length of the dumbbell specimen and became discontinuous after approximately 15% strain. As the neck gradually grew, the stress level decreased owing to a local decrease in the cross-sectional area and strain softening of the dumbbell specimen. Once the neck moves beyond its full gauge length, the stress begins to rise noticeably owing to the deformation of the high strain material and its corresponding strain hardening.[11] When strain crystallization occurs, the stress-strain curve becomes significantly steeper and the ultimate fracture strength increases. When MDH particles were introduced into PMP/PP, the elastic modulus increased slightly. Certain brittleness can be observed in samples filled with MDH, along with a decrease in strain at break. The decrease in the composite strain at break is proportional to the content of MDH particles.

Figure 4 summarizes the effect of the EB-irradiation on the tensile properties of PMP/PP/MDH composites. It can be seen that tensile strength (Figure 4(a)) and elongation at the break (Figure 4(b)) of EB-irradiated samples was slightly decreased upon EB-irradiation. In the case of PMP/PP/MDH50wt%-50Mrad, an approximately 6.4% decrease in the elongation at the break of 140% was observed relative to that of PMP/PP/MDH50wt%. The decreased tensile properties of the EB-irradiated samples may be explained by the scission of macromolecular chains induced by EB-irradiation.[12]

DSC Thermal Properties. The effect on the MDH loading level on the DSC melting and crystallization behavior of PMP/PP are shown in Figure 5 and Figure 6, respectively. The first-scan DSC thermogram of the PMP/PP sample exhibits two separate endotherms with a single melting peak at 158.2 °C, and double peaks at 208.5 and 220.2 °C in which the low-temperature peak corresponds to PP and thevhigh-temperature peak corresponds to PMP. These separate melting peaks appeared similarly for the PMP/PP/MDH composites.

The shoulder peak of the PMP phase in the first-scan DSC thermogram of unfilled the PMP/PP almost disappeared in the second-scan DSC thermogram. The shoulder of the PMP

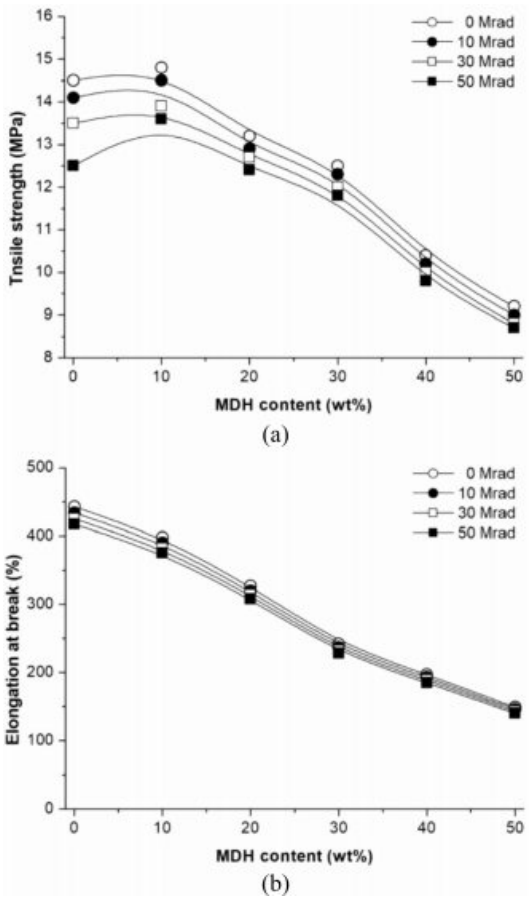

Figure 4. Effect of EB-irradiation on the tensile properties of PMP/PP/MDH composites: (a) tensile strength; (b) elongation at break

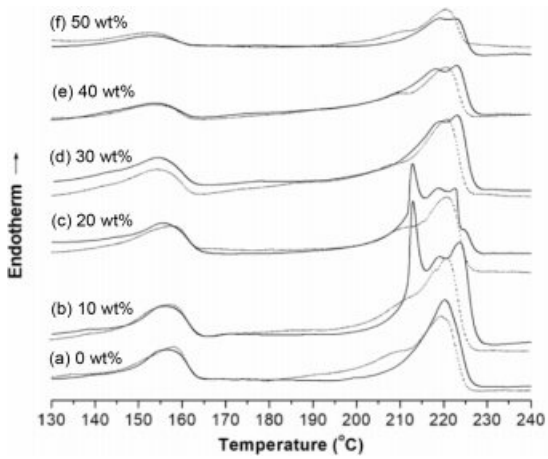

Figure 5. DSC thermograms (.....: First-scan; ____: Second-scan) of the PMP/PP/MDH composites (MDH content: (a) 0 wt%; (b) 10 wt%; (c) 20 wt%; (d) 30 wt%; (e) 40 wt%; (f) 50 wt%).

phase in the first-scan heating curve is due to the defective crystals initially formed during the quenching process. Crystals with these defects will suffer perfection in the slow cooling step. In sharp contrast all second-scan DSC curves of the PMP phase in the composites showed multiple melting behaviors. As shown in Figure 5(b), the second-scan DSC thermogram of the PMP phase in PMP/PP/MDH10wt% exhibited three distinct peaks. In the case of PMP/PP/MDH20wt%, its melting peak was split into four peaks at approximately 212.3, 212.8, 222.9 and 225.1 °C. The low-, middle-, and high-temperature peaks are ascribed to the melting of the crystals with two distinct lamellar populations.[13] It may be related to the nucleating effect of the fillers, which facilitated the formation of imperfect crystals on the surfaces of the fillers, and the perfect crystals were phase-separated during the slow cooling procedure. As the MDH content increased (> 30 wt%) the low-melting peak disappeared, and two distinct endotherms remained. This indicates that such fillers hinder the rearrangement of meta-stable polymer chains for crystallization when there are too many fillers.

Figure 6 shows the DSC cooling curves for the composites, including those of pure PMP/PP, using a -10 °C/min cooling rate. In the absence of MDH, two exotherms are present, which correspond to the sequential crystallization of PMP (at 204.9 °C) and PP (at 107.3 °C). The observed T_c values of both the PP and PMP phases in the composites decreased progressively with increasing MDH content. The drop in T_c of the PMP/PP/MDH composites with the addition of MDH suggests that it hindered the crystal growth. Additionally, multiple crystallization peaks of PMP phase appeared when 10 and 20 wt% MDH were added, which was attributed to the formation of different morphologies of the same type of crystallite.

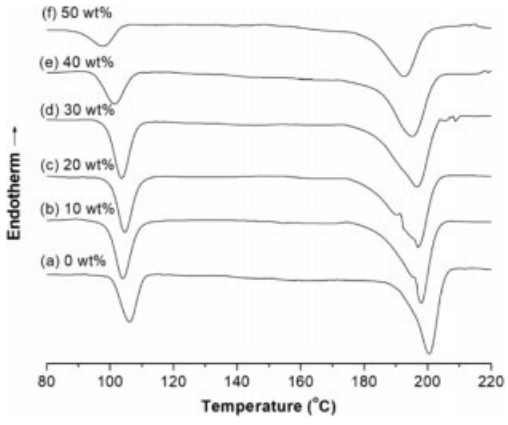

Figure 6. DSC cooling curves for the PMP/PP/MDH composites (MDH content: (a) 0 wt%; (b) 10 wt%; (c) 20 wt%; (d) 30 wt%; (e) 40 wt%; (f) 50 wt%).

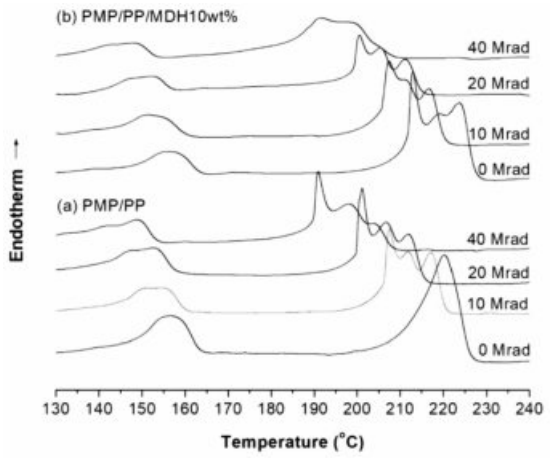

Figure 7. Second-scan DSC melting thermograms of (a) the PMP/PP; (b) PMP/PP/MDH10wt% samples before and after EB-irradiation.

Figure 7 illustrates the second-scan DSC thermograms of the PMP/PP and PMP/PP/MDH10wt% samples as a function of the EB-irradiation dose. The second-scan DSC thermograms of the PMP phase in EB-irradiated PMP/PP (Figure 7(a)) and PMP/PP/MDH10wt% (Figure 7(b)) exhibited triple endotherms. In addition the melting peaks of the PP phase of all EB-irradiated samples were split into two peaks. Crosslinking and chain scission reactions may occur in the PMP/PP sample during EB irradiation. Crosslinking and scission occur at the same time where one may predominate over the other, depending upon the irradiation dose and polymer.[12] When the film samples were irradiated by intermediate doses in air, the EB irradiation enhanced the crosslinking degree of the polymer chains, which resulted in a decrease in crystallinity. Crystallization is affected by the presence of crosslinks which reduce the chain mobility and reputation needed for lamellae to form. Consequently, the crosslinked polymer resulted in a lower degree of crystallinity compared to that of the unirradiated polymer. A competing reaction called chain-scission occurs when the polymers are EB-irradiated. In such a case, the polymer chain breaks and the molecular weight decreases. The chain scission process creates shorter polymer chain links, which make it easier to fit into a localized crystalline domain. These meta-stable molecules segregate upon cooling and produce an organized entity. The high-temperature peak may also originate from the melting of more perfect crystals formed through meta-stable phase segregation during the cooling scan.

Furthermore, it can also be seen that the peak temperature of both PP and PMP phases shift toward lower temperatures as the EB irradiation dose increases. The increased irradiation

dose causes a large accumulation of reactive intermediates such like peroxyl radicals and hydroperoxides, which promote the chain process of degradation.[14] This oxidative degradation may occur, which may produce more shortened chains, enhance crystal imperfections, and consequently lower T_m.

Thermal Stability. Figure 8 demonstrates the TGA curves of the PMP/PP/MDH composites with MDH contents of 0, 10, 30, and 50 wt%. The shapes of TGA curves indicate that the unfilled PMP/PP shows a one-step weight loss. In the case of PMP/PP, it retained 99.8% of its initial mass until the temperature reached approximately 327 °C, at which point it began to decompose. It lost 50% of its initial mass at 466 °C and lost almost all of its mass at 600 °C with a residue of 0.13% of its initial mass.

For the PMP/PP/MDH composites, the TGA traces show a gradual shift in the weight loss towards higher temperatures as the MDH content increased. The temperature at which the composite sample lost 50% ($T_{-50\%}$) of its initial mass increased with increasing MDH content. The $T_{-50\%}$ values are 466.4, 473.1, 450.1, and 513.2 °C for PMP/PP, PMP/PP/MDH10wt%, PMP/PP/MDH30wt%, and PMP/PP/MDH50wt%, for the above given order. This means that adding more MDH causes the material to decompose at a higher temperature, thereby increasing the thermal stability of the composite system. The mineral filler layer limits the transfer of oxygen and heat, which retards the thermal decomposition of the composite.[10]

The thermal decomposition curves of the PMP/PP/MDH10wt% and PMP/PP/MDH50wt% composites with different amounts of EB irradiation are shown in Figure 9. Some typical weight loss curves with temperature are shown in the figure. The thermal stabilities of the 10 and 50 wt% MDH filled composites decrease significantly with increasing radiation doses. For PMP/PP/MDH10wt%-40Mrad ($T_{-50\%}$=467.1 °C), the TGA traces show a shift of the weight loss towards lower temperature with stabilization of approximately 12 °C lower than PMP/PP/MDH10wt% ($T_{-50\%}$=479.4 °C). This confirmed that EB irradiation facilitated thermal degradation.

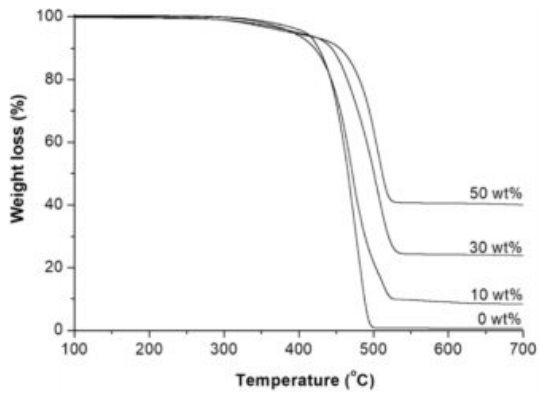

Figure 8. TGA traces of PMP/PP/MDH composites.

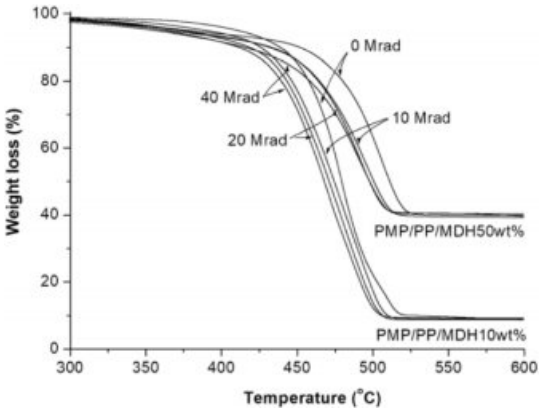

Figure 9. TGA traces of the 10 and 50 wt% MDH filled composites after EB-irradiation.

Insulation Properties. Figure 10 shows the variation in the IR in the PMP/PP/MDH composites as a function of the MDH content and EB-irradiation dose. Notably, the IR values for all composite films were higher than those of unfilled PMP/PP. The PMP/PP film exhibits an IR value of 2.74 MΩ/mm. For PMP/PP/MDH10wt% and PMP/PP/MDH50wt%, an approximately 15.2 and 2.2 % increase in the IR of 3.23 and 2.8 MΩ/mm, respectively was observed. In addition, the changes in IR showed the same tendency as that of the tensile strength of the PMP/PP/MDH composites (Figure 4(a)).

This means that the IR of the PMP/PP/MDH composite is dominated by the electric field at the tip of the defect. The maximum IR value was obtained when the MDH content was 10 wt%. As the MDH loading further increases, the IR value decreases. Micro-structural defects such as voids, cracks,

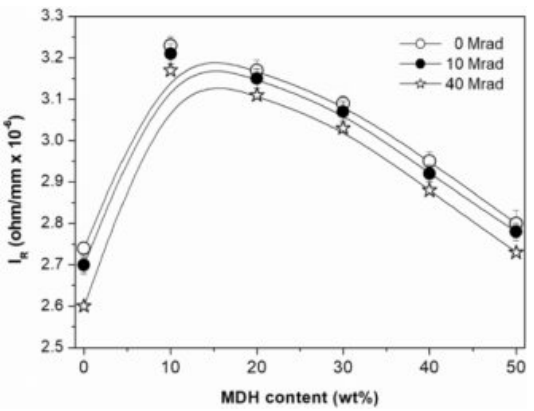

Figure 10. The variation of the insulation resistance (IR) in PMP/PP/MDH composites as a function of the MDH content and EB-irradiation dose.

delaminations, and impurities are associated with variations of IR. It is believed that the agglomeration of filler particles creates defect centers that distort and intensify the local electric field, reducing the IR value.[5] From Figure 10, all irradiated samples showed lower IR values than unirradiated samples. Crosslinking reactions at high doses occur with chain scission reactions, the latter probably predominate.[15] Thus, non-uniformities owing to molecular chain scission introduced into the polymer matrix and polar/ionic products due to EB irradiation cause a decrease in the resistance of the sample.[16]

Conclusions

The effects of MDH content on the fire, thermal, mechanical, electrical, and morphological properties of the melt-blended PMP/PP/MDH composites were examined. The incorporation of MDH significantly enhanced the flame retardancy and thermal stability of PMP/PP. However, too many of them cause the composite to become brittle and, as a result, fail at small deformations. The IR test confirmed that there was the same change tendency as the tensile strength of the PMP/PP/MDH composites, which increased up to 10 wt% MDH and then decreased thereafter. This means that the IR of the PMP/PP/MDH composite was dominated by the electric field at the tip of the defect. The introduction of MDH reduces charge accumulation, leading to an enhanced probability of electrical insulation properties. However, EB irradiation without a crosslinking agent resulted in a substantial decrease in the tensile and insulation properties and thermal stability of the PMP/PP/MDH composites. The deterioration of these properties is presumed to be an excessive dose state caused by the irradiation speed being too slow (1 m/min) or the film thickness being too thin. In the future, we plan to conduct research on optimizing the irradiation crosslinking conditions for extruded cables.

Acknowledgment(s): This work was supported by the R&D Program (JB210013) of the Korea Institute of Industrial Technology (KITECH).

Conflict of Interest: The authors declare that there is no conflict of interest.

References

1. Yong, G. J.; Lee, K. B. Development of Safety Assessment for Hydrogen Fuel Cell Vehicle. *Trans. of the Korean Hydrogen and New Energy Society* **2014**, 25, 500-508.
2. Lee, S. Y.; Seo, W. B.; Lim, J. S.; Choi, J. H. Numerical Analysis of Electromagnetic Radiation Characteristics by High Voltage and General Cables for Fuel Cell Electric Vehicle (FCEV). *Trans. of the Korean Hydrogen and New Energy Society* **2011**, 22, 152-160.
3. Fang, J.; Kiran, E. Crystallization and Gelation of Isotactic Poly(4-methyl-1-pentene) in n-pentane and in n-pentane +CO_2 at High Pressures. *J. Supercrit. Fluids* **2006**, 38, 132-145.
4. Dorigato, A.; Pegoretti, A. Tensile Creep Behaviour of Poly-methylpentene-silica Nanocomposites. *Polym. Int.* **2010**, 5, 719-724.
5. Choi, Y.-T.; Kim, S. B.; Lee, S. J.; Kim, G.-T.; Park, E.-H.; Park, E. S. Morphology, Thermal, Mechanical and Electrical Insulation Properties of Poly(4-methyl-1-pentene)/poly(ethylene-*co*-vinyl alcohol)-coated TiO_2 Nanocomposites. *Composites Part B* **2017**, 114, 268-279.
6. *Measuring the Minimum Oxygen Concentration to Support Candle-Like Combustion of Plastics (Oxygen Index)*; ASTM: West Conshohocken, PA, Sep 1, 2013; ASTM D 2863.
7. *Standard Test Methods for DC Resistance or Conductance of Insulating Materials*; ASTM: West Conshohocken, PA, Apr 1, 2014; ASTM D 257.
8. *Practice for use of a cellulose triacetate dosimetry system*; ISO/ISO: Vernier, Geneva, May 15, 2013; ASTM 51650.
9. Park, E. S. Mechanical Properties and Processibilty of Glass-Fiber-, Wollastonite-, and Fluoro Rubber- Reinforced Silicone Rubber Composites. *J. Appl. Polym. Sci.* **2007**, 105, 460-468.
10. Sałasińska, K.; Borucka, M.; Celiński, M.; Gajek, A.; Zatorski, W.; Mizera, K.; Leszczyńska, M.; Ryszkowska, J. Thermal Stability, Fire Behavior, and Fumes Emission of Polyethylene Nanocomposites with Halogen-free Fire Retardants. *Adv. Polym. Technol.* **2018**, 37, 2394-2410.
11. Sarva, S. S.; Boyce, M. C. Mechanics of Polycarbonate During High-rate Tension. *J. Mech. Mater. Struct.* **2007**, 2, 1853-1880.
12. Park, E. S. Effects of Electron Beam Irradiation on Properties of ETFE Insulated Electric Wire. *Iran Polym. J.* **2011**, 20, 873-885.
13. Wunderlich, B. Chapter IX irreversible melting. In *Macromolecular Physics*; Academic Press: New York, 1980, pp 128-191.
14. Zaharescu, T.; Silva, L. G. A.; Jipa, S.; Kappel, W. Post-irradiation Thermal Degradation of PA6 and PA6,6. *Radiat. Phys. Chem.* **2010**, 79, 388-391.
15. Valodkar, M.; Thakore, S. Thermal and Mechanical Properties of Natural Rubber and Starch Nanocomposites. *Int. J. Polym Anal.* **2010**, 15, 387-395.
16. Eyssa, H. M.; Mohamed, W. S.; El-Zayat, M. M. Irradiated Rubber Composite with Nano and Micro Fillers for Mining Rock Application. *Radiochim. Acta* **2019**, 107, 737-753.